Gas Phase dynamics of spiropyrans and spirooxazines molecules

L. Poisson, Kevin D. Raffael, Benoît Soep, Jean-Michel Mestdagh, Guy Buntin

Gas Phase dynamics of spiropyrans and spirooxazines molecules

Lionel Poisson, Kevin D. Raffael, Benoît Soep, Jean-Michel Mestdagh

Laboratoire Francis Perrin,
CEA/DSM/DRECAM/SPAM - CNRS URA 2453,
C.E.A. Saclay,
F-91191 Gif-sur-Yvette cedex, France

Guy Buntinx

Laboratoire de Spectrochimie Infrarouge et Raman (CNRS-UMR 8516)
Centre d'Etudes et de Recherches Lasers et Applications (CNRS-FR 2416)
USTL - Bât C5
F-59655 Villeneuve d'Ascq cedex, France

lionel.poisson@cea.fr

Abstract

The gas phase dynamics of two classes of photochromic molecules, three spiropyrans and one spirooxazine have been investigated here using both Time Resolved Mass Spectrometry and Photoelectron Spectroscopy approaches. It is, to our knowledge, the first gas phase experiment done of these kind of molecules. The molecules are excited at 266 nm and probed at 800 nm. The comparison of the dynamics of these four molecules has been used to propose a sequential photoisomerization mechanism involving 4 steps occurring in the first 100 ps. Each of these steps are discussed and related to the observed condensed phase dynamics and to theoretical calculations.

1 Introduction

Spiropyrans and spirooxazines are two classes of photochromic molecules, that have huge commercial applications. Spirooxazines, for example, are already used in sunlight active media and now have attracted an even greater interest for their potential as optical memories and switches.[1] For this reason, they have been largely investigated in the past, essentially in the condensed phase.[2–13]

They are of considerable interest from a molecular viewpoint since they exist under two isomeric forms that also have quite different electronic structures.[14] The nature of the mechanism that allows these molecules to switch with high efficiency from one isomeric form to another is far from being fully understood. The different absorption spectrum associated with each of the two isomeric forms and their poor overlap provides a means of monitoring experimentally the switch from one form to the other allowing a clear cut transient absorption measurement in the condense phase.

Several experimental methods have been used to retrieve information relating to the ring opening dynamics in the condensed phase: cold temperature experiments,[7] nanosecond flash photolysis experiments,[6,13,15] picosecond experiments,[16–18] and recently femtosecond experiments.[4,12,19–22] Each of these studies has provided some time constant for the evolution of the reaction within each of the time domains explored. The evidence points to a complicated mechanism involving both singlet and triplet excited states followed by solvent relaxation and thermal rearrangement.

TD-DFT calculations of Sheng *et al.*[23] provide a comprehensive mechanistic scheme for the conversion of Spiropyrans to Merocyanine in the ground state, in the lowest triplet excited state and in the singlet excited state potential energy

Regular name	nickname	CAS number
1',3'-Dihydro-1',3',3',-trimethyl-6-nitrospiro[2H-1-benzopyran-2,2'-(2H)-indole]	molecule 1	1498-88-0
1',3'-Dihydro-8-methoxy-1',3',3',-trimethyl-6-nitrospiro[2H-1-benzopyran-2,2'-(2H)-indole]	molecule 2	1498-89-1
1',3'-Dihydro-5'-methoxy-1',3',3',-trimethyl-6-nitrospiro[2H-1-benzopyran-2,2'-(2H)-indole]	molecule 3	16331-96-7
1,3-Dihydro-1,3,3,-trimethylspiro[2H-indole-2,3'-[3H]naphth[2,1-b][1,4]oxazine]	molecule 4	27333-47-1

Table 1: Name of each molecule studied and corresponding CAS number.

surfaces. These calculations were carried out for isolated molecules and then extrapolated to the condensed phase. Specifically, the conversion on excited surfaces is calculated to follow two possible pathways on the triplet surface, and only one on the singlet surface. The later involves two intermediate states: the first intermediate state corresponds to the relaxation of the excess energy to the S_1 surface of the excited spiropyran. The second, in an open structure (**TCC**), carries out a cis-trans isomerization to evolve to the structure of the Merocyanine.

At a molecular level, gas phase experiment offers the greatest chance to observe the inner building blocks of condensed phase systems in the limit where the individual molecules no longer.

Here we present femtosecond time resolved gas phase measurements on both Spiropyran and Spirooxazine molecules. Spiropyrans and Spirooxazine (see Figure 1 & Table 1) are isolated in order to reveal their inherent photodynamics, in the absence of any perturbation by a solvent and to characterize intermediates.

2 Experimental

The experimental setup used in this study will be described elsewhere,[24,25] and is summarized here (see figure 2). The source is comprised of a Parker solenoid valve

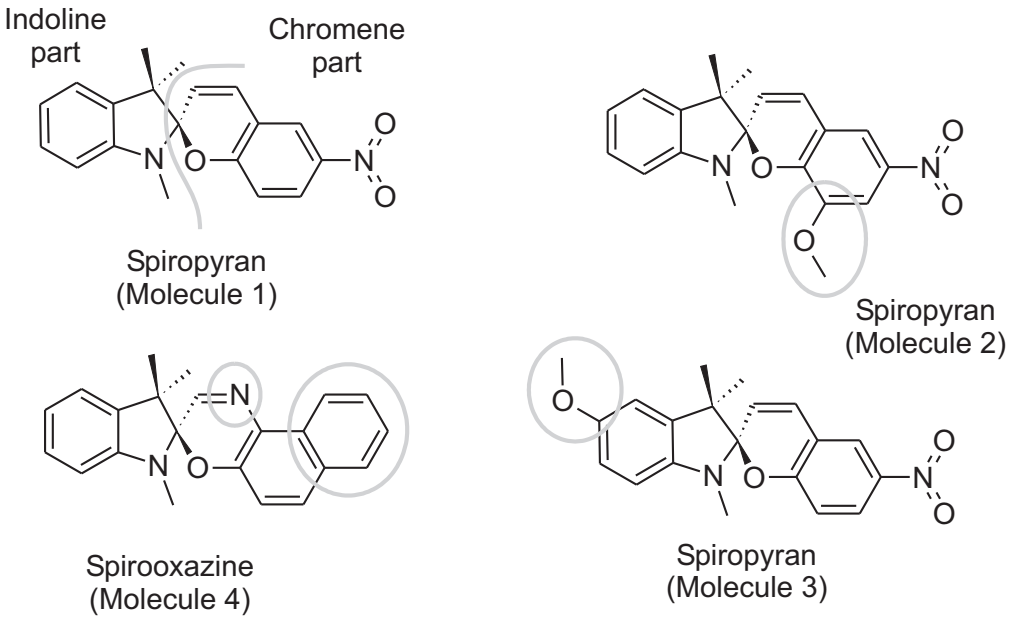

Figure 1: List of molecules investigated in this work

(formerly General Valve) with an oven mounted on the orifice plate. The oven contained the sample which was prepared by compressing a mixture of graphite and the compound of interest (see Table 1, supplied by Aldrich) into a tablet at 15 bars pressure.[26] The temperature of the oven was typically held at ∼470 K. No evidence of molecular fragmentation (or isomerization) due to source heating was observed.

The free-jet expansion was separated from the region of interaction by a skimmer. Molecules entrained in the carrier gas helium, held at ∼2 bar stagnation pressure, were probed perpendicularly to the beam axis by a femtosecond laser (LUCA, a European SLIC facility). In accordance with the typical absorption spectra for the molecules of interest, the third harmonic of the Ti:sapphire laser (267 nm) was used as the pump pulse. Following the initial excitation, the fundamental of

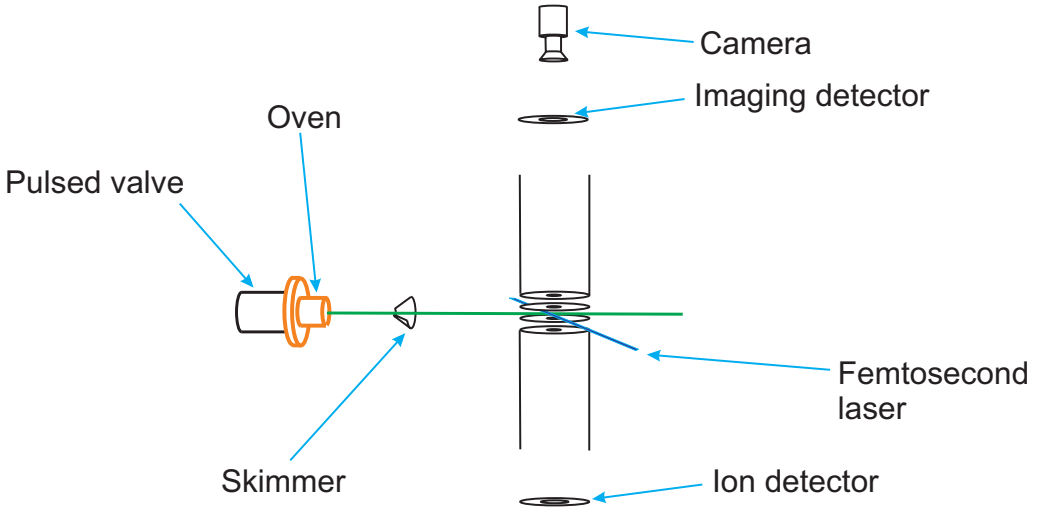

Figure 2: Schematic of the experimental setup

the Ti:sapphire (800 nm) was used as the probe pulse in a multiphoton ionisation process.

Two sets of electrodes were used to extract electrons and ions from the zone of interaction. The first set, uniquely used for ion detection, forms a Wiley-McLaren Time-of-Flight device in which ions are detected using microchannel plates. The second set of electrodes belongs to a Velocity Map Imaging (VMI) device (based on the developments of A. T. J. B. Eppink and D. H. Parker[27,28]) which enables electrons or ions over a full 4π solid angle to be detected. Using this technique, electrons or ions are projected onto a position sensitive detector which is then monitored by a close circuit camera. Data are accumulated by summing the resultant images. The distributions depend on the velocities of the charged particles so that it is possible to derive the kinetic energy of the fragment ions or the ejection energy of electrons by an analysis of the images collected. The Hansen and Law algorithm[29] which is based on an inverse Abel Transform is used to reconstruct

the original expanding ion or electron volume which is spherically symmetric if no inherent anisotropy exists.

Low energy ions and electrons are especially well-resolved by this technique. However, since information is extracted from an angular distribution spread over an area, a greater number of averages must be recorded to achieve equivalent signal to noise ratios as obtained by ordinary mass spectrometry. This drawback is partially compensated for by a 4π steradian collection of the charged particles.

The energy calibration of the photoelectron images (which can in turn be used to calibrate ion energies) was carried out by introducing Xe and Ar into the ionization chamber. For the length of flight tube and the extraction voltages used in the present study, the calibration was $E(eV) = (8.6 \pm 0.8) \cdot 10^{-5} \cdot \mathrm{r}^2$, where r is the distance from the center of the image (expressed in numbers of pixels). Note the r scale is proportional to the particle velocity. Instrument parameters and data collection were controlled by a program written in LabVIEW. For relatively short relaxation dynamics (of the order of a few picoseconds) the pump-probe delay was randomly set from a predetermined list of values over the course of each experiment; this allowed laser intensity fluctuations to be more easily identified amongst recorded signals. Each pump-probe delay range was repeated several times so that largely differing signals could be eliminated from the final summation. Relatively long time dynamics (several tens or hundreds of picoseconds) were monitored by stepping the pump-probe delay over a range in a forward fashion and then in a backward fashion for the following series. Variable pump/probe step size permitted the scanning of dynamics with small increments in the neighborhood of zero delay providing a point of reference for the comparison of all dynamics. An average of 1000 to 1500 laser shots per pump/probe delay was used to generate the

time-of-flight spectra and the electron images.

3 Results and data analysis

As is commonly observed in an experiment involving photoionization, several fragment ions appear beside the molecular mass of the parent. This raises the question of whether the fragment ions result from the ionization of an excited neutral fragmenting during the time interval between the pump and the probe, or from a fragmentation of the molecular ion. Hence, before presenting the pump/probe results and their analysis, we present mass spectra and discuss the origin of the observed fragment peaks.

3.1 Mass spectrum and assignment of the fragment ions

A typical mass spectrum for molecule 1 (see figure 1) is displayed in figure 3. The truncated signal at 322 g.mol^{-1} corresponds to the parent whilst the relatively sharp peak at 175 g.mol^{-1} is attributed to an impurity in the sample. The other peaks are attributed to fragment ions. The width of the parent peak is comparable to that of the impurity at half maximum when the full scale is observed. In contrast, those of the fragments are significantly broader. This is good evidence that the peaks below the mass of the parent ion signal derive from a fragmentation process.

It can be reasoned in a number of ways that the cation fragments detected in these experiments are generated at the time of ionization or following ionization:

- Energy conservation: a photoion image of the mass at 159 g.mol^{-1}, which is

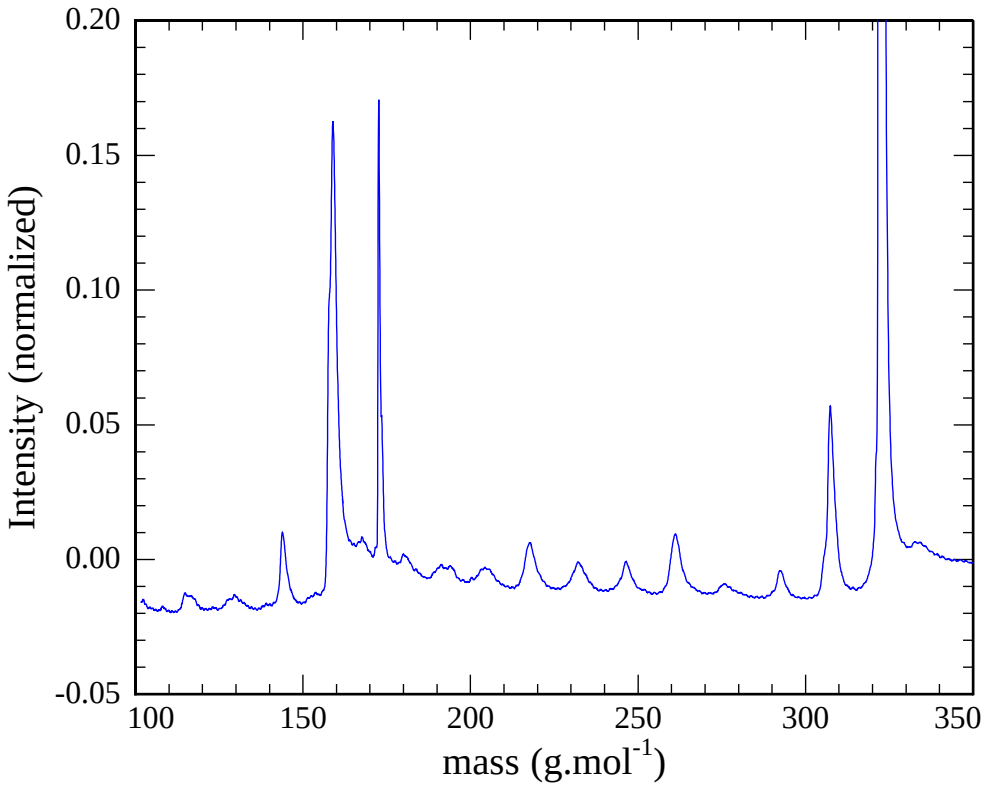

Figure 3: Mass spectrum of molecule 1 for 266 nm pump/800 nm probe summed over -0.5 ps to 1.5 ps, pump/probe delay

approximately half the molecular mass of the parent, shows this fragment, to have translational energy of 0.7 eV. Conservation of momentum requires that equal energy leaves with the remaining half (whether in one or several fragments) so that the total translational energy is approximately ∼1.4 eV. If the neutral is excited at 266 nm (4.65 eV) approximately 3.3 eV of energy will be available for fragmentation in the neutral molecule. This does not represent sufficient energy to break both the C-C and C-O bonds necessary to give rise to the observed fragmentation.

- Rise time: further evidence for different fragments being generated after ion-

ization of the parent molecule is drawn from the observed pump-probe rise times for parent and fragment ions. No shift is observed between the parent and fragment appearance times and later dynamics resemble one another closely. Differences in intensities relate to the changing dissociation cross sections favoring particular dissociation channels. For example, an increase in the dissociation cross section described above, is indicative of the opening of the pyran cycle as it induces a fragility in the molecule.

- Furthermore, the photoion-VMI fragment energy distribution does not show any dependence on pump-probe delay time.

At a first glance the observation of either the parent or the fragment pump-probe signal should carry the same information on the excited state dynamics. However, the nature of the fragment pump-probe signal carries additional information on the structure of the excited molecule at the time of ionization. This signal is related to the branching ratio between non fragmentation and fragmentation by the probe laser. For this reason only the parent and the principal fragment ions are considered here. The structure of the principal fragment from each of the four molecules is given in figure 4. It consists of the indoline subunit and the corresponding substituent (see table 2).

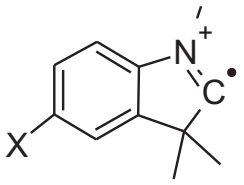

Figure 4: Structure of the most abundant fragment. X = −H for all molecules but molecule 3 where X = $-O-CH_3$.

Molecule	mass g.mol^{-1}	supposed formula (see figure 4)
molecule 1	≈ 159	$X = -H$
molecule 2	≈ 159	$X = -H$
molecule 3	≈ 190	$X = -O - CH_3$
molecule 4	≈ 159	$X = -H$

Table 2: Mass of the largest fragment which is attibuted to the indoline part of the photochroms.

To our knowledge there are no ionization potentials (IP) reported for any of the molecules studied in the present paper. We can nevertheless estimate the IPs by considering the molecules as composed of two independent orthogonal delocalized systems; an indoline subunit and a chromene subunit as shown in figure 1. These subunits are only covalently connected and little or no electron delocalisation is expected to occur between them. Thus, in a first approximation we will consider each subunit independently and estimate the effect of their substituents on the IP. The following values have been obtained from the NIST webbook[30,31] by averaging the values from PE experiment or by using the evaluated values when available.

The indoline subunit, 2,3-dihydro-1H-Indole (CAS 496-15-1) has an IP of 7.15 eV. The addition of several donor electrons groups to this molecule is expected to stabilize the ion and to lower the IP. For example the 2,3-dihydro-1,3,3-trimethyl-2-methylene-1H-indole (CAS 118-12-7) has an IP of 6.98 eV. Hence, we can estimate the IP of the indoline subunit to be about 7.0 eV (see figure 5). The effect of the addi-

tion of a para-methoxy group can be estimated by the difference between the IP of the 4-methoxy-N,N-dimethyl-benzenamine (CAS 701-56-4) and the N,N-dimethyl-benzenamine (CAS 121-69-7) that gives $6.7 - 7.12 \sim -0.4$ **eV. For the Chromene subunit 2,2-dimethyl-2H-1-**

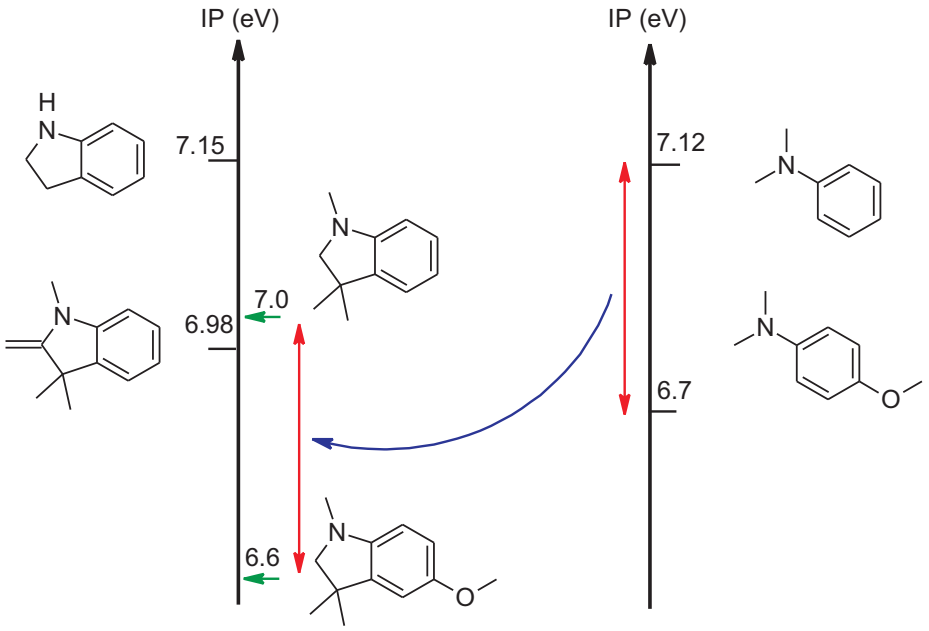

Figure 5: Method used for the estimation of the IP's for the Indoline subunit.

Benzopyran (CAS 2513-25-9) can be considered as a reasonable approximation, with an IP of 7.8 eV. According to the IP difference between 1-methoxy,4-nitrobenzene (CAS 100-17-4) and methoxybenzene (CAS 100-66-3) the effect of a paranitro group on the IP is roughly $8.9 - 8.32 \sim +0.6$ **eV. The same calculations are performed for the naphtooxazine unit of molecule 4 and are given in Table 3.**

It appears in Table 3, that in the ground state of the parent ion for all the molecules studied here, the positive charge would be expected to

Molecule	chromene subunit	indoline subunit
molecule 1	$\sim$ 8.4 eV	$\sim$ 7.0 eV
molecule 2	$\sim$ 8.0 eV	$\sim$ 7.0 eV
molecule 3	$\sim$ 8.4 eV	$\sim$ 6.6 eV
molecule 4	$\sim$ 7.4 eV	$\sim$ 7.0 eV

Table 3: Rough estimation of the ionization potential for each subunit. Details of the calculation are presented in the text. The accuracy is $\sim$ 0.2 eV

be located on the indoline subunit.

3.2 Pump/probe experiments

Relatively fast dynamics (0 - 2 ps) and slower dynamics (up to 200 ps) were observed for each of the four molecules under consideration by following the evolution of both photoelectron and mass spectra as a function of pump-probe delay time.

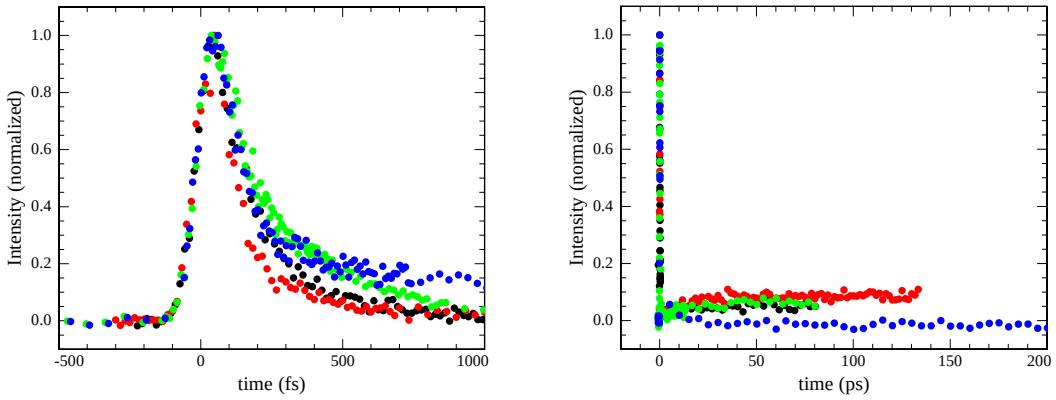

Figure 6: Normalized time pump/probe signals for the parent mass for two time scales. Black corresponds to molecule 1, red to molecule 2, green to molecule 3 and blue to molecule 4.

The pump-probe signals for the four parents and principal fragments are shown

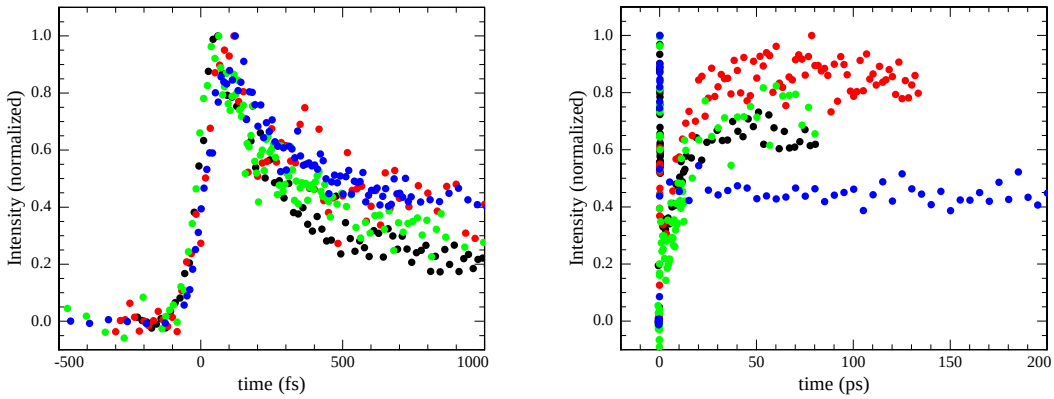

Figure 7: Normalized pump/probe signals of the fragment mass (see table 2) over two time scales. Black corresponds to molecule 1, red to molecule 2, green to molecule 3 and blue to molecule 4.

in figures 6 and 7. The time evolution of each mass appears to show three time components. This is more visible in figure 7. The left diagram shows a distinct biexponential behavior for molecule 1 with one decay time lower than 100 fs and the other of the order of 500 fs. The right diagram shows a slower rise of the order of 20 ps. The simplest linear kinetic model that is appropriate to describe such relaxation dynamics is a step cascade of the form:

$$\text{Form A} \xrightarrow{\tau_1} \text{Form B} \xrightarrow{\tau_2} \text{Form C} \xrightarrow{\tau_3} \text{Form D} \tag{1}$$

Where Forms A $\cdots$ D are labels involving no implication upon the nature of their molecular structure or their electronic excitation. As we shall see in the discussion, such a scheme can be related to the TD-DFT calculations of Sheng *et al.*[23] The kinetics for this model gives rise of the following rate equations:

$$C_{\text{Form A}}(t) = C_0 \exp\left(-\frac{t}{\tau_1}\right) \quad (2)$$

$$C_{\text{Form B}}(t) = \frac{C_0}{\left(\frac{1}{\tau_2}-\frac{1}{\tau_1}\right)\tau_1}\left(\exp\left(-\frac{t}{\tau_1}\right)-\exp\left(-\frac{t}{\tau_2}\right)\right) \quad (3)$$

$$C_{\text{Form C}}(t) = \frac{C_0}{\tau_1-\tau_2}\left[\frac{1}{\frac{1}{\tau_3}-\frac{1}{\tau_1}}\left(\exp\left(-\frac{t}{\tau_1}\right)-\exp\left(-\frac{t}{\tau_3}\right)\right)-\frac{1}{\frac{1}{\tau_3}-\frac{1}{\tau_2}}\left(\exp\left(-\frac{t}{\tau_2}\right)-\exp\left(-\frac{t}{\tau_3}\right)\right)\right] \quad (4)$$

$$C_{\text{Form D}}(t) = \frac{C_0}{(\tau_1-\tau_2)\tau_3}\left[\frac{1}{\frac{1}{\tau_3}-\frac{1}{\tau_1}}\left(\tau_1\left(1-\exp\left(-\frac{t}{\tau_1}\right)\right)-\tau_3\left(1-\exp\left(-\frac{t}{\tau_3}\right)\right)\right)-\frac{1}{\frac{1}{\tau_3}-\frac{1}{\tau_2}}\left(\tau_2\left(1-\exp\left(-\frac{t}{\tau_2}\right)\right)-\tau_3\left(1-\exp\left(-\frac{t}{\tau_3}\right)\right)\right)\right] \quad (5)$$

Where C_0 is the initial amount of molecule excited to Form A. The time profiles corresponding to these rate equations are plotted in figure 8. Each form corresponds to a different electronic state or a different conformation of the molecule and is expected to have different ionisation and/or fragmentation cross sections as is apparent in the observed pump-probe signals. Thus four cross sections are incorporated as multiplying factors to fit the experimental data. Since only relative intensities for each form are determinable in the present study and not absolute cross sections - only their relative values can be derived in the fit. Hence, the pump-probe delay signals for the masses considered can be fitted to three rate constants and three cross sections with the forth held constant. The cross section of Form B (σ_B) was set to unity since the contribution to the pump-probe signal from Form B gave the least uncertainty between observed and simulated dynamics. Since the time scales for each of the three dynamical components are appreciably different the fits to the experimental curves can be done with good accuracy. As described above, parent and fragment ion signals are associated with the same

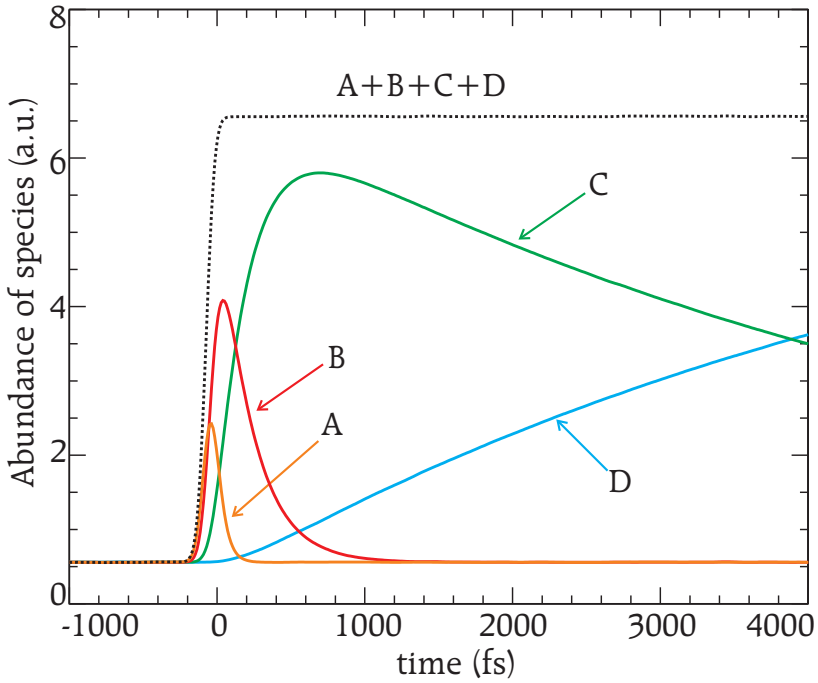

Figure 8: Relative abundance of the different species. These functions form the basis set of functions for the fit of the experimental results (figure 6 and figure 7). The respective decay times τ_1, τ_2 and τ_3 used in this example are 47 fs, 213 fs and 5333 fs.

dynamics and are fitted to the same set of curves and the same time constants. The signals have been fitted by the function $Fit(t)$ that is a convolution product of the function $f(t)$ and a gaussian function $g(t)$ - the cross correlation profile of the laser. For each mass the fit function is therefore defined as:

$$
\begin{aligned}
Fit(t) &= (f * g)(t - \gamma) \qquad (6)\\
f(t) &= \alpha\left(\sigma_A C_{\text{Form A}}(t) + 1 \cdot C_{\text{Form B}}(t) + \sigma_C C_{\text{Form C}}(t) + \sigma_D C_{\text{Form D}}(t)\right) + \beta\\
g(t) &= \frac{2\ln(2)}{\delta\sqrt{\pi}} \exp\left(-\frac{\ln(2)t^2}{(\delta/2)^2}\right)
\end{aligned}
$$

β (y offset), γ (t offset) and δ (laser pulse width at half maximum) can be

Molecule	Ionization of molecule				Ionization & formation of fragment			
	σ_A	σ_B	σ_C	σ_D	σ_A	σ_B	σ_C	σ_D
molecule 1	4.35	1.00	0.24	0.09	2.39	1.00	0.30	0.70
molecule 2	9.10	1.00	0.007	0.25	0.80	1.00	0.26	0.72
molecule 3	3.57	1.00	< 0.002	0.10	2.04	1.00	0.22	0.74
molecule 4	4.17	1.00	0.24	< 0.002	0.60	1.00	0.38	0.38
Accuracy	$\pm$ 10%	N/A	$\pm$ 10%	$\pm$ 5%	$\pm$ 10%	N/A	$\pm$ 10%	$\pm$ 5%

Table 4: Cross sections of parent ionization (without fragmentation) referenced to the cross section of Form B, and the ionization of the parent followed by the formation of the fragment represented in figure 4.

found with much higher precision than rate and cross section parameters and are not dependent on the dynamics. δ is fixed to 110 fs for all fit functions. The results of the fits are presented in tables 4 and 5.

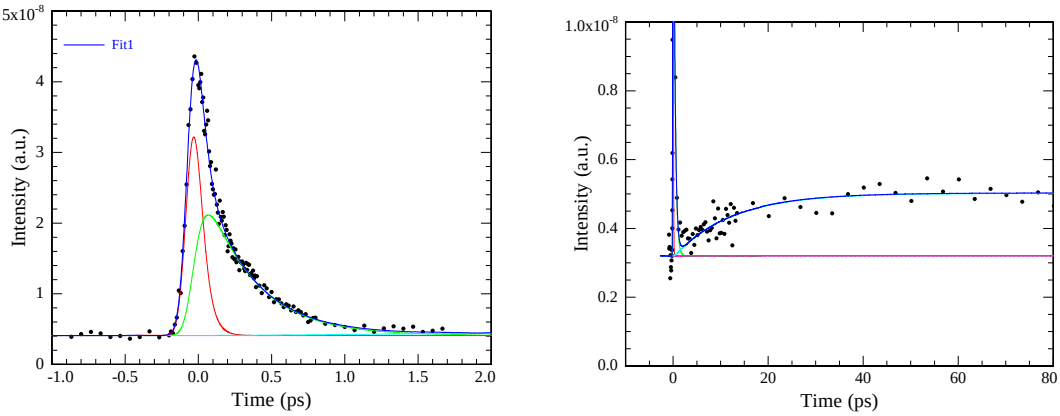

Figure 9: Fit obtained with molecule 3 at the parent mass, using equation 6 with the parameters presented in tables 4 and 5.

3.3 Photoelectron spectroscopy

General considerations: The photoelectron spectroscopy provides us with an additional information to the mass spectra only if the ionization

Molecule	τ_1(fs)	τ_2(fs)	τ_3(fs)
molecule 1	40	233	12,000
molecule 2	43	267	12,000
molecule 3	47	333	12,000
molecule 4	47	213	5,300
Accuracy	± 3%	± 3%	± 7%

Table 5: Time constants given by the fit of the experimental data for all the molecules studied.

process observed is a direct ionization. In that case, the energy of the electrons ejected while probing the observed state yields information on the electronic state at a given pump/probe delay. In the case of an electronic or vibrational autoionization, the energy of the ejected electron observed is only related to the overlap between the potential energy surfaces of the superexcited autoionizing state and the ion, which has little relation to the excited state dynamics of interest.

Practically, in the very approximate case of an excitation by the pump of a monoelectronic orbital where the electron to be removed is localized on the same atom as the charge in the ion, the ionization is direct and well-described by the Koopman's theorem,[32] with almost no configuration change before ionization. In the alternative case where a vibrationally induced configuration change is necessary for ionization to take place, autoionization will occur. These two extreme cases can appear successively when ionizing an excited neutral species that evolves with time. This is typically what would be expected in a "complementary

Koopmans' type correlation" as that introduced by Stolow *et al.*[32–34] but in a particular case where the probe laser can ionize only one of the two states concerned, and reach a Rydberg state for the other one. The autoionized electron is ejected in a delay that can be greater than the picosecond.

In the present case an extensive molecular fragmentation can observed in figure 3. With two almost independent cycles, the electronic autoionization may play an important role. Indeed, as the excitation may be localized on one subunit of the molecule, the probe laser can either ionize the excited subunit or excite the other. The total energy involved is the same, but the second process induces a fast electronic autoionization[32,35] where the excess energy is partially relaxed to the vibrational modes instead of being converted into electron kinetic energy.

Because of the number of fragmentation channels involved and the complexity of the ionization mechanism, a structureless broad photoelectron spectrum independent of the ionization energy[36] is observed. If it is assumed that electrons are principally ejected from the parent then the number of vibrational and electronic states populated in the remaining ion population can be evaluated by considering the number of fragment ions observed in the mass spectrum.

Present study: A time dependent photoelectron spectrum for each molecule was recorded using 266 nm as the pump and 800 nm as the probe in order to further characterize the evolution of the excited neutrals.[37] The important features of the electron spectra along the re-

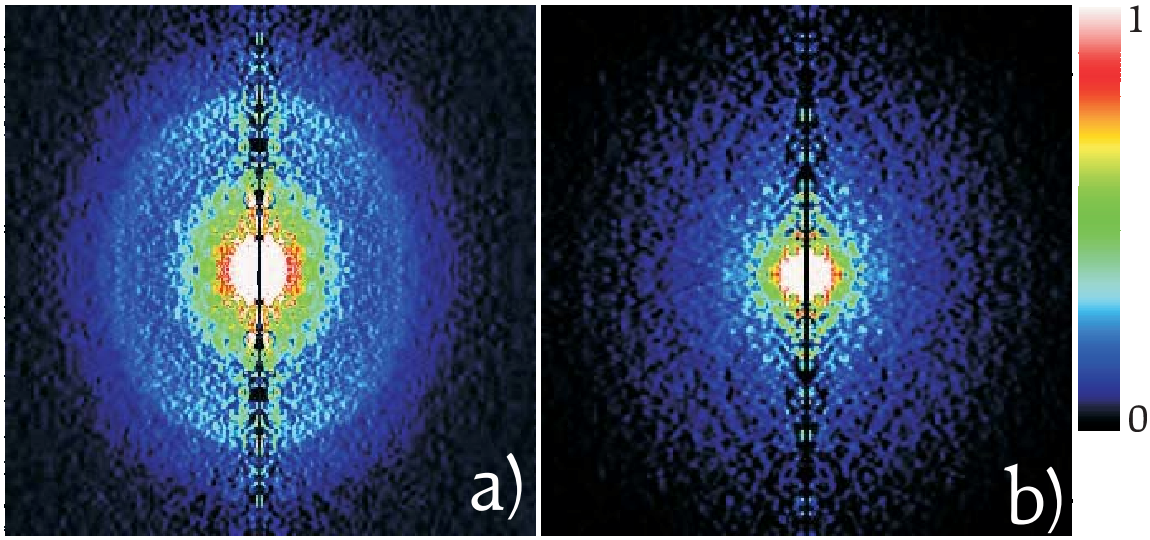

Figure 10: Photoelectron images of molecule 3 obtained for a pump/probe (266 nm/800 nm) experiment, inverted and summed for a) short times delays ($t < 3\ ps$), b) long time delays ($3\ ps < t < 200\ ps$).

action path of the excited neutral molecules are recorded by summing electron images collected for different pump-probe delays over the time interval of interest, as shown in figures 10 and 11. The following is observed:

- The photoelectron spectra have similar structures for the molecules in this study.
- There is a structural feature for short time delays peaking at $\sim 0.55\ eV$.
- **The short time delay feature for molecule 3 appears broader at the higher electron energies (figure 11) when compared to molecule 1 and 2 which share the same skeleton. The feature for molecule 3 drops at about 1 eV, whilst it falls off at about 0.75 eV for molecule 1 and 2.**

- This feature disappears for longer time delays.
- **The polarization of the structural feature shown in figure 10 is fitted by a second order Legendre polynomial. Higher order terms are negligible.**

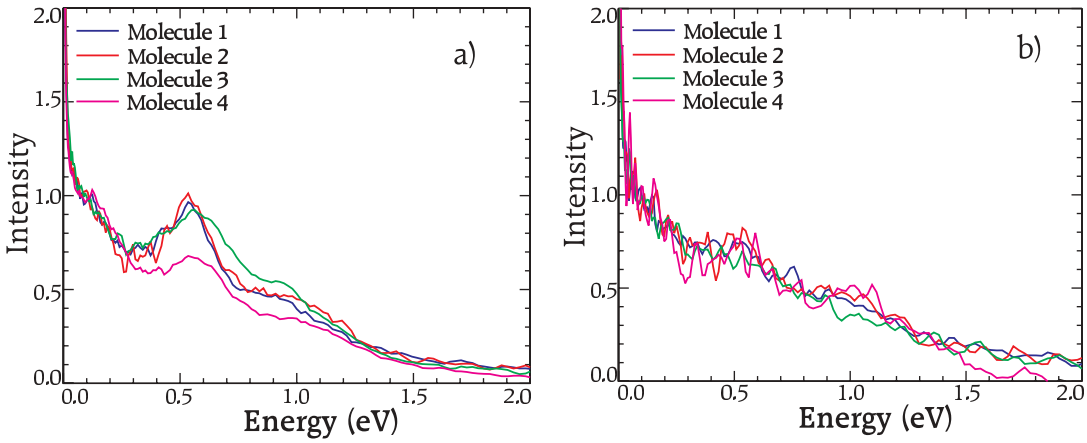

Figure 11: Normalized photoelectron spectra for all molecules from a) the sum of images obtained in the pump/probe experiment (266 nm/800 nm) for short time delays ($t < 3\ ps$), b) the sum of images obtained under the same conditions as a) but at longer time delays ($3\ ps < t < 200\ ps$).

Figure 12 shows photoelectron spectra for molecule 3 for images summed over different pump-probe delay regions where Form A is predominant, around the maximum of Form B and when Form C is less contaminated by the other forms. These regions were selected from the evolution of the parent pump-probe signal. It is apparent that the structural feature in the photoelectron spectrum is greatest when Form B is most predominant.

The feature observed while Form B is most present corresponds to a structure expected for a direct ionization process. The polarization of the feature gives us information on the initial electronic state convoluted by probe ionization. However, because of the multiphoton character of

this ionization, the geometry of the initial state is not determinable. According to the previous discussion, it appears that the structure of Form B should be similar to that of the ion. Furthermore, the difference observed for molecule 3 suggests that this state is localized on the indoline subunit.

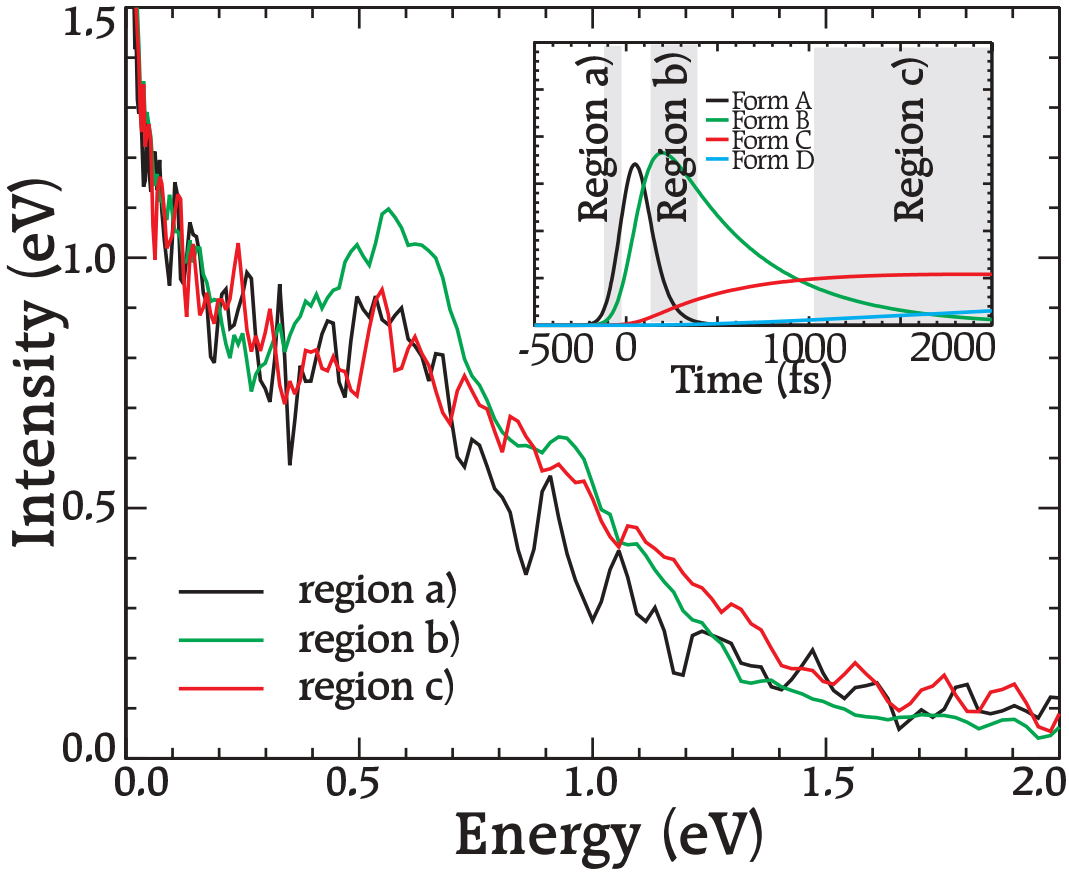

Figure 12: Photoelectron images of molecule 3 summed for different regions and normalized, superimposed for low energies. The insert presents the result of the fit for the formation of the fragment of molecule 3. It appears that the structure at $0.55 \pm 0.5\ eV$ is higher when Form B is at a maximum.

4 Discussion

The kinetic model (1) emphasises the four forms (labelled A to D) that are sequentially populated by the excited molecules under investigation. At this point, Forms A to D are simply labels that do not presume any electronic state or any particular conformation. Of course Form A represents the electronic state of each molecule that is populated by the vertical excitation from the pump laser. We attempt to identify the localization of this initial electronic excitation. Forms B to D must be completely characterized electronically and geometrically. The best approach with this purpose in mind is to compare the behavior of the 4 molecules for a given form. We will reason within a relaxation scheme in which the pyran cycle opens and then allows the double bond to twist to generate form D. We shall use dynamical and theoretical arguments to justify the mechanism summarized in figure 13.

4.1 Form-to-Form discussion

Form A: We already saw that all of the studied molecules presented in figure 1, are composed of two independent orthogonal delocalized systems; an indoline subunit and a chromene subunit. From Table 5 it appears that the decay of Form A is about the same, $\sim$ 45 fs, for each of the molecules. However Table 4 shows a contrast in the relative intensity of Form A (σ_A) for molecule 2 where it is twice that of molecule 1 and 3 which have the same spiropyran skeleton. Furthermore, the cross sections for both ionization and fragmentation are very low for molecule 2 when compared to molecule 1 and 3 which are similar. This suggests that the initial excitation is located on the chromene subunit (right part) of the

4 molecules studied (see Figure 1). **This observation is also supported by absorptions experiments conducted by Tyler *et al.*[38,39] Comparison of the absorption spectra of each independent subunit of the molecules and the absorption spectra of the spiropyrans indicates that the S_1 state and the S_3 state which absorbs around 266 nm are located on the chromene subunit.**

Form B: Photoelectron spectra are shown in Figures 12 & 10. In the time interval where Form B appears, the photoelectron spectrum for all molecules exhibits a common feature. This indicates the population of a similar excited state present in all four molecules. There is one possible localization of the electronic excitation common to all molecules: the common central part of the molecules. The structure at ~ 0.55 eV grows with the abundance of Form B. The relatively well resolved nature of this feature suggests a state localized close to the electronic defect of the ion configuration. **According to the estimation of the IP in table 3 this state might be a Rydberg state of a series converging toward an ion with the charge located on the Indoline subunit. Form B is generated very quickly: 40-47 fs. On the other hand, previous studies of some phenolic molecules or biomolecules in which a phenol or an aniline core is present[40,41] suggest the possibility of a rapid $^1\pi\pi^\star$ to $^1\pi\sigma^\star$ relaxation. In the phenol case, the $\sigma^\star$ is located on the $\Phi O - H$ bond. If we assume that the excited state is localized on the chromene subunit, modeled here by a substituted phenolic subunit, and involves some Rydberg character, the mechanism resembles that involved for Phenol and Azines by Sobolewski *et al.*,[40] but on a $\Phi O - C$ bond. Here the $^1\pi\sigma^\star$ localization with Rydberg character is thought to result in dis-**

sociation. According to the photoelectron spectrum, we can attribute Form B to the state $^1\pi\sigma^\star$ in each of the molecules, *i.e.* to an anti-bonding electronic state that will induce the opening of the spirospyran or spirooxazine cycle. Indeed, this anti-bonding orbital is principally localized on the carbon atom, that is strongly coupled to the lone pair of electrons of the closeby Nitrogen atom. The corresponding ion has the same geometrical structure as the fragment presented in figure 4. Because of the Rydberg character of this state, its electronic energy difference with the ion is almost independent of the substituent. As seen previously, the photoelectron energy grows at 0.55 eV and extends up to 0.75 eV for molecule 1 and 2 while it extends up to 1 eV for molecule 3. According to the IPs given in table 3, the features are in complete agreement with an ionization by 2 photons at 800 nm that increases the total excitation energy up to 7.75 eV. As the IP of molecule 3's indoline subunit is slightly lower than that of the others (6.6 eV instead of 7.0 eV) the photoelectron spectrum looks warmer. The dissociation time is then given by the time τ_2 in table 5. It appears to be between 213 to 333 fs. Due to the anti-bonding electron, this bond rupture is expected to evolve to a biradical electronic structure.

Form C: The contributions as depicted in figure 7 and 8 shows that Form C is almost undetected despite its appearance over a significant time domain. This is reflected in the low values of σ_C. One possibility is that the IP of Form C is higher relative to Forms A, B or D. **Since the IP of the molecule is given by the indoline side, this suggests some change in the indoline subunit that increases the IP. An electron transfer, from the C radical, originating**

from the $C-O$ bond rupture, to the chromene subunit is stabilized on one hand by the lone pair of the nearby Nitrogen, and on the other hand by the strong electron affinity (EA) of the chromene subunit (expected to be even greater than the EA of the phenolic radical ~ 2.25 eV[42]). The Zwitterion has the positive charge localized on the indoline subunit which can, thus, not be further ionized. The negative charge is delocalised on the chromene subunit. This delocalization induces some geometry changes in the hole subunit that may explain the broad photoelectron spectrum. The decay time, τ_3, of Form C is very similar for the spiropyrans molecules, 1 to 3, (12 ps for molecule 1, molecule 2 and molecule 3), but is different for the spirooxazine (5.3 ps). One interpretation could be that Form C corresponds to the isomerization of the double bond from the cis to the trans form: The isomerization process in spirooxazine may involve a smaller angle change (120° for an inversion mechanism) with no rupture of the π electronic system of the $C=N$ double bond.[43] This facilitates the isomerization in relation to the mechanism involving with the $C=C$ double bond requiring a 180° torsion.

Form D: Form D is the last detected within the time scale studied. It has a higher detection cross section than Form C (σ_D, Table 4), and a broad photoelectron spectrum (Figure 10 & 11) at least for the three spiropyrans. Molecule 4 will be discussed in a later paragraph. This suggests the recovery of a neutral electronic state. This may be induced by an electronic "connection" between the two subunits. Furthermore, the ionization cross sections for each of the spiropyrans is lower than the ionization and fragmentation process leading to the formation of the indoline ion. This is what would be expected from the ionization of a structure with an open pyran cycle. Indeed, the fragmentation of a closed pyran cycle

requires the rupture of two bonds whilst the fragmentation of the open cycle requires only one rupture. These arguments suggest an attribution of Form D to a merocyanin-like structure. The open structure in the ground state has a high absorption cross section at 400 nm. Therefore the observation of an absorption by a probe at 800 nm is in support of this open structure existing in an excited state. Furthermore, a pump-probe experiment at 266 nm/400 nm did not show any dramatic improvement in the absorption cross section of Form D. We did not see any depletion of signal for Form D. We estimate its lifetime to be greater than 500 ps for each of the molecules studied. We note that no evidence for the formation of the more stable, cis/trans, isomer is found in this study.

Figure 13 represents the summary of the attributions discussed.

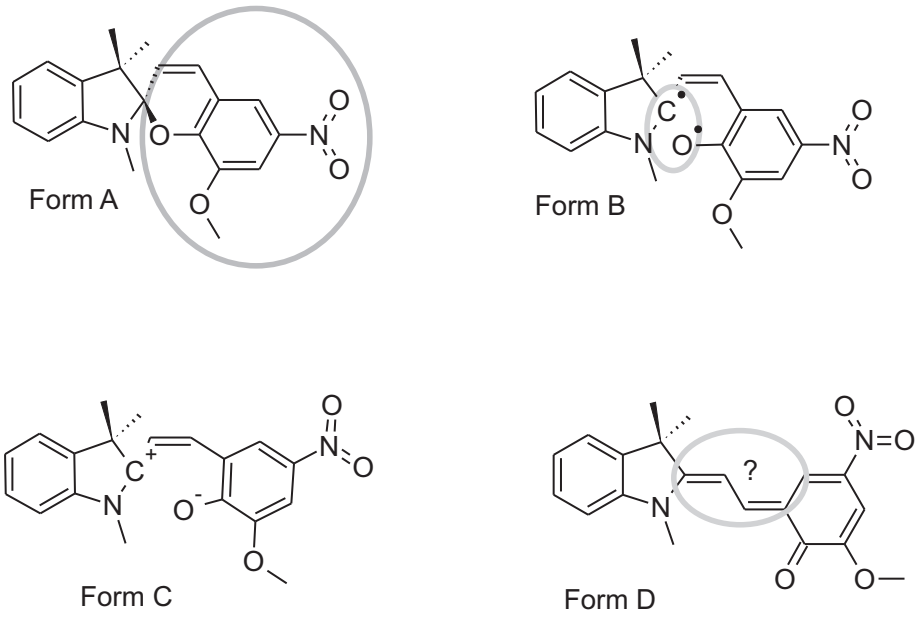

Figure 13: Four structures attributed to the different steps of the observed dynamics represented here for molecule 2. The circles indicate the dynamically active part of each Form. The isomeric structure of Form D is speculated.

4.2 Mechanism

The model presented here is a tentative one. However, support for this mechanism is given by theoretical calculations.[23]

The kinetic model proposed here (equation 1) can be compared to other models found in the literature and inferred on the basis of condensed phase dynamical studies.[4] Femtosecond excitation in the liquid phase reduces the time resolution due to wavelength dispersion in the solvent such that the shortest time constant (< 100 fs) is more difficult to access. We expect the liquid phase studies to reveal only one Form whereas Forms A and B are resolved in these gas phase experiments. On the other hand, the ground state of the parent was not accessible in these experiments, because of its high ionization energy; any energy relaxation from the excited state to the ground state is not detected. The presence of an intermediate state on the ground state PES in this relaxation process is also not observed in this study while it can be observed in the liquid phase. The scheme described using the observations of liquid phase experiments is as follows:

$$\begin{aligned} \text{Form A} \xrightarrow{\tau_0'} \text{Form C} \xrightarrow{\tau_3'} \text{Form D} \\ \xrightarrow{\tau_1'} \text{Form E} \xrightarrow{\tau_2'} \text{Ground State} \end{aligned} \tag{7}$$

where τ_x' are the inverse of the rate constant. Our model is consistent with the condensed phase observations, but not with all aspects of the model given in the literature. According to the calculations of Sobolewski *et al.*[41] on small aromatic molecules, relaxation to the ground state most likely proceeds from the Form B that is not considered in the models given for the condensed phase studies.

It is important to notice here that the presence of a relaxation channel, not considered in our model, is also incorporated in σ_X that actually represents the product

of the absolute cross section and the number of molecules.

Evidence has been given for a sequential mechanism. The principal uncertainty is, however, associated with the appearance of Form B. Its sequential appearance is confirmed by the late increase in the feature of the photoelectron spectrum associated with Form B.

4.3 Singlet vs Triplet electronic state

Condensed phase experiments have shown that the triplet state can play a role in the dynamics of spyropyrans and spirooxazines[6,44] especially when substituted with nitrated groups. The participation of this state depends on the degree of substitution.[45] On the other hand, unsubstituted spiropyrans and spyrooxazines are known to commute only in the singlet state,[13,46] even if the triplet pathway exists and can be accessed indirectly by photoactivation of the benzophenone.[47]

The calculations done by Sheng *et al.*,[23] show a reaction pathway represented by the following scheme:

$$\mathbf{SP}^{\star} \longrightarrow {}^{x}\mathbf{SP} \longrightarrow {}^{x}\mathbf{TCC} \longrightarrow {}^{x}\mathbf{TTC} \tag{8}$$

where **SP** refers to the spiropyran molecule, and **TCC** and **TTC** refer to the configurations trans- and cis- of the three $C-C$ bonds linking the indoline to the phenol part of the merocyanin molecule. There appears to be a clear relationship between Form A and $\mathbf{SP}^{\star}$, Form B and ${}^{x}\mathbf{SP}$, Form C and ${}^{x}\mathbf{TCC}$ and Form D and ${}^{x}\mathbf{TTC}$.

Based on energetic arguments of the barriers, the authors of this theoretical paper conclude that for strong donor-acceptor substituted spiropyrans the isomerization takes place exclusively on the triplet-state PES.

The substituent of the three spiropyrans molecules studied here has both strong

donor (NO_2)-acceptor ($N-CH_3$) characters. According to the condensed phase literature and the TD-DFT calculations, the molecules 1 to 3 have dynamics which involve excited triplet states whereas molecule 4 is not expected to.

There, it is suggested that Form B is created from the singlet Form A in less than 50 fs and transformed to Form C in less than 350 fs. On account of the short time scales involved, it is considered unlikely that the Forms A and B have a triplet character. This is further supported by the singlet character of the states involved in the $^1\pi\pi^\star$ to $^1\pi\sigma^\star$ relaxation described in the literature.[41] Furthermore, Sheng *et al.*[23] presents two possible pathways for a transformation to the merocyanin structure via a triplet state, and only one via the singlet state, on the grounds of barrier heights. We have not found any evidence for the presence of two mechanisms for this transformation. However, the techniques used in this investigation are not sufficiently sensitive to small deviations in the dynamic profile.

If we compare the set of molecules which are considered as having a triplet state involved in the dynamics *i.e.* molecule 1, 2 and 3 with molecule 4 which is thought to isomerize in the singlet state, we note that the ionization cross section, σ_D, is 0 for molecule 4 and greater than σ_C for each of the other molecules. Here, it is not clear whether this indicates that molecule 4 has relaxed to the fundamental state in a singlet state mechanism or whether this is a result of some characteristic difference between the spirooxazine and the spiropyran skeleton. If we suppose that Form D is the triplet state for the nitro-spiropyrans and the fundamental state for the spirooxazine, it suggests that τ_3 is the conversion time. Then, it is not clear why this time is longer for the conversion to the triplet state than for the conversion to the ground state. The inverse is expected. The questions also stay open for Form C and Form D, and further investigation is needed.

4.4 Effect of substituents

The present study does not permit a complete understanding of the substituent effects since they usually give rise to minor energy changes at the equilibrium geometry and the transition state. The total energy introduced in the molecule by these femtosecond pulses is much higher than the transition state energy considered. Furthermore, the signal observed, depends on the number of molecules irradiated, on the absolute excitation cross section, the absolute ionization cross section of the excited molecule in each Form and on the laser intensity. Since, we do not have access to the initial molecular number density, all the absolute ionization cross sections are indeterminate.

Nevertheless the role of the substituent can be observed within the time constants in Table 5 where there are no dramatic differences observed between molecules 1, 2 and 3.

According to our interpretation and to Sobolewski *et al.*,[41] the transient efficiency is ensured by the presence of a substituent that allows the relaxation from $^1\pi\pi^\star$ to $^1\pi\sigma^\star$ (especially in the gas phase). The substituent may also play a role in which relaxation to the ground state through a conical intersection is avoided thus favoring the intersystem crossing to a triplet state.

5 Conclusion

We have studied the time resolved gas phase dynamics of several spiropyrans and spirooxazines differing by minor functional groups. The comparison of their dy-

namics and their ionization cross sections has helped us to verify a sequential mechanism where four steps have been observed. We have been able to characterize two of these, although questions still remain unanswered for the others. The first step (Form A) is assigned to the initial excited state ($^1\pi\pi^\star$). This state is depleted into Form B attributable to $^1\pi\sigma^\star$ in about $\sim$50 fs. Form B evolves in $\sim$260 fs to Form C which is presumed to have its pyranic cycle opened and to be in the process of isomerizing. The analysis of time resolved photoelectron spectra lends credence to the assignment of Form B to the $^1\pi\sigma^\star$ state and the low of ionization efficiency of Form C and its assignment to an open structure zwitterion. Form D is created from Form C in $\sim$10 ps. We assume that the electronic connection between both subunits is recovered in this step and that this form has a structure close to the merocyanin structure.

In the future, we plan to study another set of molecules selected to resolve the question of the actual excited states involved in the dynamics. A further study will focus on the influence of a solvent on the relaxation process, by depositing the photochromic molecule on a large argon cluster and then by introducing solvent molecules. Matrix isolation studies should be helpful for the full characterization of the Form C.

Acknowledgments

The authors are happy to thank O. Gobert, the late P. Meynadier, M. Perdrix, F. Lepetit, J.F. Hergott and D. Garzella who are responsible for the developing, maintaining and running of the femtosecond laser facility LUCA (Laser Ultra-Court Accordable) of the CEA, DSM/DRECAM. This work is partly supported by the European Community through the PICNIC network (Product Imaging

and Correlation: Non-adiabatic Interactions in Chemistry) under contract number HPRN-CT-2002-00183.

References

1. Berkovic, G.; Krongauz, V.; Weiss, V. *Chemical Reviews* **2000,** *100,* 1741-1753.
2. Minkin, V. I. *Chemical Reviews* **2004,** *104,* 2751-2776.
3. Lokshin, V.; Samat, A.; Metelitsa, A. V. *Russ. Chem. Rev.* **2002,** *71,* 893-916.
4. Rini, M.; Holm, A. K.; Nibbering, E. T. J.; Fidder, H. *J. Am. Chem. Soc* **2003,** *125,* 3028-3034.
5. Ernsting, N. P.; Arthen-Engeland, T. *J. Phys. Chem.* **1991,** *95,* 5502-5509.
6. Lenoble, C.; Becker, R. S. *J. Phys. Chem.* **1986,** *90,* 62-65.
7. Heiligman-Rim, R.; Hirshberg, Y.; Fischer, E. *J. Phys. Chem.* **1962,** *66,* 2470-2477.
8. Suzuki, M.; Asahi, T.; Takahashi, K.; Masuhara, H. *Chem. Phys. Lett.* **2003,** *368,* 384-392.
9. Khairutdinov, R. F.; Giertz, K.; Hurst, J. K.; Voloshina, E. N.; Voloshin, N. A.; Minkin, V. I. *J. Am. Chem. Soc* **1998,** *120,* 12707-12713.
10. Cottone, G.; Noto, R.; La Manna, G. *Chem. Phys. Lett.* **2004,** *388,* 218-222.
11. Hobley, J.; Pfeifer-Fukumura, U.; Bletz, M.; Asahi, T.; Masuhara, H.; Fukumura, H. *J. Phys. Chem. A* **2002,** *106,* 2265-2270.
12. Zhang, J. Z.; Schwartz, B. J.; King, J. C.; Harris, C. B. *J. Am. Chem. Soc* **1992,** *114,* 10921-10927.
13. Kellmann, A.; Tfibel, F.; Guglielmetti, R. *J. Photochem. Photobiol. A: Chem.* **1995,** *91,* 131-136.
14. Irie, M. *Chemical Reviews* **2000,** *100,* 1683-1683.

15. Tamaki, T.; Sakuragi, M.; Ichimura, K.; Aoki, K. *Chem. Phys. Lett.* **1989,** *161,* 23-26.

16. Aramaki, S.; Atkinson, G. H. *J. Am. Chem. Soc* **1992,** *114,* 438-444.

17. Wilkinson, F.; Worrall, D. R.; Hobley, J.; Jansen, L.; Williams, S. L.; Langley, A. J.; Matousek, P. *Journal of the Chemical Society-Faraday Transactions* **1996,** *92,* 1331-1336.

18. Schneider, S.; Mindl, A.; Elfinger, G.; Melzig, M. *Ber. Bunsenges. Phys. Chem.* **1987,** *91,* 1222-1224.

19. Holm, A. K.; Rini, M.; Nibbering, E. T. J.; Fidder, H. *Chem. Phys. Lett.* **2003,** *376,* 214-219.

20. Tamai, N.; Masuhara, H. *Chem. Phys. Lett.* **1992,** *191,* 189-194.

21. Antipin, S. A.; Petrukhin, A. N.; Gostev, F. E.; Marevtsev, V. S.; Titov, A. A.; Barachevsky, V. A.; Strokach, Y. P.; Sarkisov, O. M. *Chem. Phys. Lett.* **2000,** *331,* 378-386.

22. Buntinx, G.; Foley, S.; Lefumeux, C.; Lokshin, V.; Poizat, O.; Samat, A. *Chem. Phys. Lett.* **2004,** *391,* 33-37.

23. Sheng, Y. H.; Leszczynski, J.; Garcia, A. A.; Rosario, R.; Gust, D.; Springer, J. *Journal of Physical Chemistry B* **2004,** *108,* 16233-16243.

24. Gloaguen, E. *Photodynamique de systèmes complexes,* Thesis, Université Paris XI, 2005.

25. Gloaguen, E.; Mestdagh, J. M.; Poisson, L.; Lepetit, F.; Visticot, J. P.; Soep, B.; Coroiu, M.; Eppink, A. T. J. B.; Parker, D. H. *J. Am. Chem. Soc.* **2005,** *127,* 16529-16534.

26. Shafizadeh, N.; Krim, L.; Sorgues, S.; Soep, B. *Chem. Phys. Lett.* **2002,** *357,* 37-44.

27. Eppink, A.; Parker, D. H. *Review of Scientific Instruments* **1997,** *68,* 3477-3484.

28. Whitaker, B. J. *Imaging in Molecular Dynamics : Technology and Applications;* Cambridge University Press: Cambridge, 2003.

29. Hansen, E.; Law, P.-L. *J. Opt. Soc. Amer.* **1985,** *2,* 510.

30. Lias, S.; Levin, R.; Kafafi, S. Ion Energetics Data. In *NIST Chemistry WebBook, NIST Standard Reference Database*, Vol. Number 69; Linstrom, P.; Mallard, W., Eds.; National Institute of Standards and Technology: Gaithersburg MD, 20899, 2005.

31. Lias, S.; Bartmess, J.; Liebman, J.; Holmes, R.; Levin, R.; Mallard, W. Ion Energetics Data. In *NIST Chemistry WebBook, NIST Standard Reference Database*, Vol. Number 69; Linstrom, P.; Mallard, W., Eds.; National Institute of Standards and Technology: Gaithersburg MD, 20899, 2005.

32. Pratt, S. T. *Radiation Physics and Chemistry* **2004,** *70,* 435-452.

33. Blanchet, V.; Zgierski, M. Z.; Stolow, A. *J. Chem. Phys.* **2001,** *114,* 1194-1205.

34. Schmitt, M.; Lochbrunner, S.; Shaffer, J. P.; Larsen, J. J.; Zgierski, M. Z.; Stolow, A. *J. Chem. Phys.* **2001,** *114,* 1206-1213.

35. Taylor, D. P.; Goode, J. G.; LeClaire, J. E.; Johnson, P. M. *J. Chem. Phys.* **1995,** *103,* 6293-6295.

36. Lee, S.-H.; Tang, K.-C.; Chen, I.-C.; Schmitt, M.; Shaffer, J. P.; Schultz, T.;

Underwood, J. . G.; Zgierski, M. Z.; Stolow, A. *J. Phys. Chem. A* **2002,** *106,* 8979-8991.

37. Stolow, A.; Bragg, A. E.; Neumark, D. M. *Chemical Reviews* **2004,** *104,* 1719-1757.

38. Tyer, N. W.; Becker, R. S. *J. Am. Chem. Soc* **1970,** *92,* 1289-1294.

39. Tyer, N. W.; Becker, R. S. *J. Am. Chem. Soc* **1970,** *92,* 1295-1302.

40. David, O.; Dedonder-Lardeux, C.; Jouvet, C. *Int. Rev. Phys. Chem.* **2002,** *21,* 499-523.

41. Sobolewski, A. L.; Domcke, W.; Dedonder-Lardeux, C.; Jouvet, C. *Phys. Chem. Chem. Phys.* **2002,** *4,* 1093-1100.

42. Gunion, R. F.; Gilles, M. K.; Polak, M. L.; Lineberger, W. C. *Int. J. Mass Spec. Ion Proc.* **1992,** *117,* 601-620.

43. Schultz, T.; Quenneville, J.; Levine, B.; Toniolo, A.; Martinez, T. J.; Lochbrunner, S.; Schmitt, M.; Shaffer, J. P.; Zgierski, M. Z.; Stolow, A. *J. Am. Chem. Soc* **2003,** *125,* 8098-8099.

44. Sakuragi, M.; Aoki, K.; Tamaki, T.; Ichimura, K. *Bull. Chem. Soc. Jpn.* **1990,** *63,* 74-79.

45. Kellmann, A.; Tfibel, F.; Pottier, E.; Guglielmetti, R.; Samat, A.; Rajzmann, M. *J. Photochem. Photobiol. A: Chem.* **1993,** *76,* 77-82.

46. Kellmann, A.; Tfibel, F.; Dubest, R.; Levoir, P.; Aubard, J.; Pottier, E.; Guglielmetti, R. *J. Photochem. Photobiol. A: Chem.* **1989,** *49,* 63-73.

47. Bercovici, T.; Fischer, E. *J. Am. Chem. Soc* **1964,** *86,* 5687-5688.

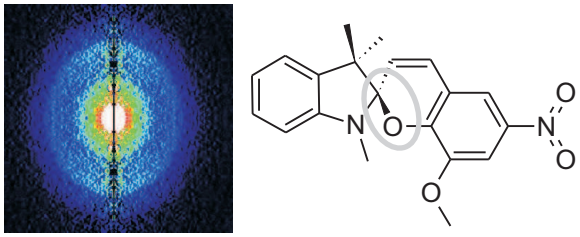

TOC graphic